Nanoscale

PAPER

View Article Online
View Journal | View Issue

Cite this: *Nanoscale*, 2014, **6**, 8117

Catalytic degradation of dye molecules and *in situ* SERS monitoring by peroxidase-like Au/CuS composite†

Qian Cai, Shunkai Lu, Fan Liao, Yanqing Li,* Shuzhen Ma and Mingwang Shao*

Received 1st April 2014
Accepted 20th May 2014

DOI: 10.1039/c4nr01751j

www.rsc.org/nanoscale

In this paper, Au/CuS composites were fabricated by a two-step method based on a facile solvothermal approach combined with the *in situ* reduction. It was demonstrated that the Au/CuS composite not only exhibited excellent peroxidase-like catalytic activity in the oxidation of the typical peroxidases (*o*-phenylenediamine and diaminobenzidine), but also showed promising SERS performance with remarkable sensitivity and high reproducibility. Based on these properties, the bi-functional Au/CuS composite was employed both as a catalyst for degrading a pollutant (Rhodamine 6G) and a SERS substrate for real-time monitoring of the degradation process quantitatively.

1. Introduction

With the rapid development of dyestuff industry, an enormous amount of industrial dye waste produced during industrial processes has led serious threats to microorganisms, aquatic environments and human beings.[1–4] Therefore, increasing attention has been paid to the degradation of industrial dyes. Many remediation strategies such as adsorption, reverse osmosis, ultrasonic decomposition, chemical oxidation, and catalytic degradation, have been proposed for the purification of industrial wastewater.[5–9] Among them, hydrogen peroxide (H_2O_2) catalytic oxidation, producing highly reactive hydroxyl radicals with catalysts of metal oxides or sulfides, has been proven to be an effective method for treating dye-containing wastewater.[10,11]

UV-visible absorption spectroscopy was generally used to monitor the catalytic reaction process in previous studies.[12,13] However, UV-visible absorption spectroscopy is not surface-selective, which provides only limited chemical information. Thus, it suffers from the limitation of the broad spectrum with low sensitivity and high demand for solution's transparency.[14,15]

As a powerful and attractive spectroscopic technique, surface-enhanced Raman spectroscopy (SERS) is becoming a quite helpful tool for the detection of organic pollutants with rapid response, high sensitivity and the capability to provide real-time molecular level vibrational information.[16–18] Compared with UV-visible spectroscopy, SERS offers attractive merits for applications in monitoring the catalytic reactions. The most prominent characteristic is that it can acquire the unique fingerprints of the molecules on the surface of the catalyst up to single-molecule sensitivity and reflect the real catalytic process.[14]

To apply SERS technology in monitoring catalytic reactions, it is necessary to synthesize the materials possessing not only catalytic activity but also SERS activity. Actually, most catalysts are constituted by SERS-inactive materials. Recently, various nanocomposites were fabricated to overcome this problem. In these cases, the combination of semiconductors and noble metals has attracted attention due to their promising applications both in catalysis and SERS fields.[19–22] Moreover, dielectric semiconductor substrate can interact with metal particles and the permittivity of the composite material is responsible for strong scattering, which is of great importance to SERS.[23,24]

Here, a SERS-active substrate made of copper sulfide nanoplate–Au nanoparticle (Au/CuS) composite was fabricated, which had the bi-function of the catalytic degradation and real-time SERS detection of organic pollutants. It is reported that Au nanoparticle is a common SERS substrate, which could dramatically enhance the Raman signals of molecules adsorbed onto the gold surface.[25,26]

As one of the important transitional metal chalcogenide semiconductors, CuS raises considerable concerns due to its potential applications in various fields, such as photocatalysis,[27] solar-cell devices,[28] optical limiting and biosensors.[29] Recently, a series of three-dimensional CuS with hierarchical structures have been proved to own intrinsic peroxidase-like catalytic activity similar to Fe_3O_4 magnetic nanoparticles.[30–32] These Fenton-like reagents could degrade organic dyestuff into non-toxic small molecules (CO_2 and H_2O) in the presence of hydrogen peroxide by releasing hydroxyl radicals with high

Institute of Functional Nano & Soft Materials (FUNSOM), Jiangsu Key Laboratory for Carbon-based Functional Materials and Devices & Collaborative Innovation Center of Suzhou Nano Science and Technology, Soochow University, Suzhou 215123, P. R. China. E-mail: mwshao@suda.edu.cn; yqli@suda.edu.cn; Fax: +86 512 65882846; Tel: +86 512 65880953

† Electronic supplementary information (ESI) available. See DOI: 10.1039/c4nr01751j

reactivity.[33,34] Thus, the peroxidase activity had a wide range of practical applications, such as the ability to catalyze the oxidation of organic substrates to decrease their toxicity and/or chromaticity, which was frequently used for wastewater treatment or as a detection tool.[35,36]

In this paper, a facile solvothermal method was reported to fabricate CuS nanoplate-based hierarchical structures, and the Au nanoparticles were then *in situ* reduced onto the surface of CuS nanoplates. Based on these qualifications, the Au/CuS composite exhibited both highly efficient peroxidase-like catalytic activity and excellent SERS performance. Therefore, the bifunctional Au/CuS composites were suitable for *in situ* real-time degradation and monitoring of the dye pollutants.

2. Experimental section

2.1 Materials

All chemical reagents were of analytical grade and used without further purification.

2.2 Preparation of CuS nanoplate-based architectures

A sophisticated solvothermal method was used to synthesize CuS. In a typical procedure, 2 mmol $Cu(NO_3)_2 \cdot 3H_2O$ and 0.35 g cetyltrimethyl ammonium bromide were dissolved in 20 mL glycol. The sulfur powder (4 mmol) in 20 mL glycol was then added dropwise under constant magnetic stirring. The mixture was then transferred into a 50 mL Teflon-lined stainless-steel autoclave. The autoclave was sealed and maintained at 160 °C for 8 h, and then cooled to room temperature naturally. Finally, the as-formed black precipitates were centrifuged and washed several times sequentially with deionized water and ethanol, and dried under vacuum at 60 °C for 6 h.

2.3 Preparation of Au/CuS substrate

First, the as-prepared CuS nanoplates (0.3 g) were dispersed in 30 mL deionized water by ultrasonicating for 15 min. 2 mL $HAuCl_4$ (10 g L^{-1}) solution was then slowly dropped into CuS solution under vigorous stirring, followed by the addition of ammonia to adjust the pH value to 10. The $HAuCl_4$ was reduced to Au nanoparticles by adding 3 mL ascorbic acid (10 mM). The solution color changed from black to pale purple-red. Under vigorous agitation for 4 h, the products were collected by centrifugation, washed with deionized water and ethanol, and then dried at 60 °C for 6 h under vacuum.

2.4 The measurement of peroxidase-like activity of Au/CuS composites

The catalytic oxidation of *o*-phenylenediamine (OPD) and diaminobenzidine (DAB) by Au/CuS composites in the presence of H_2O_2 was performed in the following manner: 800 μL of 30% H_2O_2 and 400 μL of 15 mM OPD (freshly prepared) or DAB were added to 20 mL deionized water. 2 mg as-prepared Au/CuS composites were then dispersed in 10 mL deionized water with the assistance of ultrasonic irradiation. The oxidation progress was initiated once the Au/CuS suspensions were added to the above-mentioned mixture. The catalytic oxidation progress was monitored at 1 min intervals by recording the absorption spectra.

2.5 Finite-difference time-domain (FDTD) simulation

The FDTD simulation was performed with the program FDTD Solutions (version 7.5.1), a product of Lumerical Solutions, Inc., Vancouver, Canada. A nanostructure composed of two Au nanoparticles (16 nm diameter) with the gap of 2 nm laid on the surface of CuS nanoplate with dimension of 500 nm × 500 nm × 40 nm. The dielectric constant of Au was taken from the report of Palik, whereas the dielectric constant of CuS was calculated in the ESI.† The incident beam was a total field-scattered field source of light, consisting of plane waves. Boundary conditions were imposed using the perfectly matched layer method. The electrical field distribution in the vicinity of the nanostructures was evaluated by a set of frequency domain field profile monitors. The simulations were run for a period of 1000 fs in all the cases, whereas the mesh size of 0.2 nm was chosen for calculation.

2.6 SERS monitoring and degradation of Rhodamine 6G (R6G)

The SERS monitoring and degradation were processed in a liquid system. First, the Au/CuS substrate was prepared by dropping Au/CuS aqueous solution on the clear Si wafer. After drying naturally, the Au/CuS substrate was placed in a quartz cell of 400 μL. The R6G aqueous solution (200 μL, 2×10^{-5} M) was added into the groove and covered with a quartz coverslip. The groove was then placed on the sample stage of the Raman spectroscope. In the process of Raman detection, the laser (633 nm) was focused on the surface of the Au/CuS composites through the quartz window. The SERS signals were collected with 1 min intervals once the diluted H_2O_2 ($H_2O_2 : H_2O = 1 : 1$) was added into the solution.

2.7 Characterization

The as-prepared products were characterized by X-ray diffraction (XRD, a Philips X'pert PRO MPD diffractometer) with Cu Kα radiation ($\lambda = 0.15406$ nm) and a scanning rate of 0.05° s^{-1}. The morphology and size of the products were examined by field emission scanning electronic microscopy (FESEM, FEI Co., model Quanta-200). The transmission electron microscopy (TEM) and high-resolution transmission electron microscope (HRTEM) images were taken with an HRTEM analyzer (FEI Tecnai G2 F20) with an accelerating voltage of 200 kV. Spectroscopic properties were recorded by an ultraviolet (Evolution 220), fluorescence (PL, FLWOROMAX-4, HORIBA) and Raman spectrometers (LabRAM HR 800 Raman spectroscope, J Y, France). The spectrograph uses 600 g mm^{-1} gratings and a 633 nm He–Ne laser with a power intensity of about 4 mW. SERS spectra were collected at a 50× objective (Olympus) with a numerical aperture (NA) of 0.5 and an integration time of 1 s. The laser size (d) focused on the sample is 1.54 μm according to the formula $d = 1.22\lambda/NA$,[37] where λ is the laser wavelength.

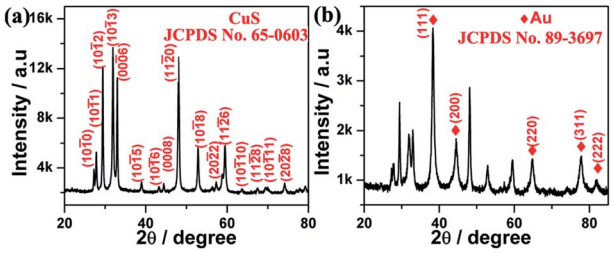

Fig. 1 XRD patterns of (a) as-prepared CuS products and (b) Au/CuS composites.

3. Results and discussion

3.1 Structure and morphology

Fig. 1(a) presents the XRD pattern of the as-prepared samples from the solvothermal method. All the diffraction peaks in the pattern can be indexed to pure hexagonal phase CuS (JCPDS Card no. 65-0603) with the $P6_3/mmc$ space group and a primitive unit cell with $a = 0.37851$ and $c = 1.62969$ nm.

The morphology of the as-prepared CuS products was characterized by SEM. A low-magnification image of CuS is shown in Fig. 2(a). It clearly reveals that the well dispersed samples are composed of uniform CuS hierarchical architectures with the diameters in the range of 500–700 nm, and the architectures are made up of nanoplates. From the high-magnification image in Fig. 2(b), the nanoplate is the shape of a hexagon with the thickness of 30–50 nm and an edge length of about 300 nm.

Fig. 1(b) displays the XRD pattern of the Au-decorated CuS samples. All the other peaks could be attributed to the cubic phase Au (JCPDS Card no. 65-0603) besides the peaks of the hexagonal phase CuS. Moreover, the strong peaks of Au (111), (200), (220) and (311) also revealed that the Au content in the decorated CuS nanoplates is quite high. In addition, the mass content of Au was about 16.7 wt%, according to the semi-quantitative analysis of the diffraction data (details in the ESI†).[38,39]

The morphology of Au/CuS composites was investigated by SEM and TEM. No significant variation on the morphology of CuS was observed from the SEM image in Fig. 3(a) when an abundance of Au nanoparticles were decorated on the surface of CuS nanoplates. The low-magnification TEM image (Fig. 3(b)) further proved that the Au nanoparticles were successfully reduced onto the surface of CuS nanoplates. The average size of Au particles can be acquired from the size distribution

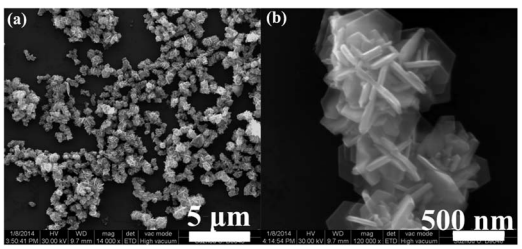

Fig. 2 SEM images of as-prepared CuS products with (a) low magnification and (b) high magnification.

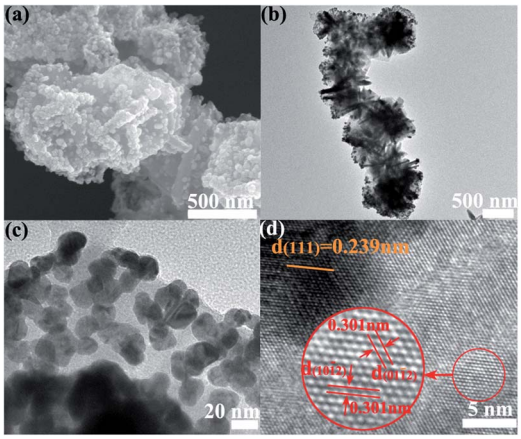

Fig. 3 (a) SEM image, (b) low-magnification TEM image, (c) high-magnification TEM image, and (d) HRTEM image of the Au/CuS composites.

histogram (Fig. S1†) based on 50 particles from the high-magnification image of the TEM (Fig. 3(c)). The size basically presents the Gauss normal distribution, which is 15.97 nm with the standard error of 0.167. Fig. 3(d) displays the HRTEM image of the sample. Two identical lattice spacings (shown in the inset) of 0.301 nm can be relatively assigned to the (10−12) and (01−12) planes of the hexagonal CuS, respectively. On the left part of the image (orange line), the lattice spacing of $d = 0.239$ nm is consistent with the (111) plane of cubic Au.

3.2 FDTD simulation

The electrical field distribution was first simulated by FDTD solution before the Au/CuS composite being used for SERS detection. FDTD is a numerical analysis technique used to simulate the distribution of the electromagnetic field around the illuminated nanoparticles, tips and substrates in the SERS system with arbitrary geometry.[40,41] The dielectric constant of the material is an important parameter for FDTD simulation. Therefore, the real and imaginary parts of the CuS dielectric constant are calculated using the data, including the absorption coefficient, optical band gap value and the refractive index (see ESI†).[42,43]

According to these dielectric constant data, the simulation (Fig. 4) revealed that the electric field enhancement localized

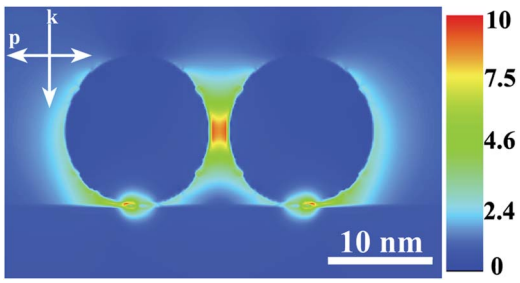

Fig. 4 The distribution of the electric field for Au/CuS composites calculated with FDTD simulation (k is the orientation of the incident light, and p is the direction of polarization).

not only in the interparticle between the Au nanoparticles, but also the gap between Au nanoparticles and CuS nanoplate. It is verified that SERS enhancement for metal nanoparticles is mainly caused by the local surface plasmon resonance effect, which leads to a strongly enhanced electric field on the surfaces of metal nanostructures.[44] Thus, it can be assumed that not only the large electromagnetic (EM) field coupling between the Au nanoparticles but also the EM coupling between Au nanoparticles and CuS nanoplates would lead to high SERS activity. Briefly, the FDTD simulation also suggested that the Au/CuS composite would be a good substrate for SERS enhancement.

3.3 SERS performance of Au/CuS composites

To evaluate the SERS performance of the Au/CuS substrate, Raman experiments were conducted by employing R6G as the probe molecule owing to its well-established vibrational features.[26] The Au/CuS substrate was placed in a quartz cell of 400 μL, and 200 μL 1×10^{-6} M R6G aqueous solution was then added into the groove. The substrate exhibited remarkable SERS activity as seen from the upper part of Fig. 5. The main vibrations of R6G for the aromatic C–C stretching modes[45] at 1307, 1359, 1507 and 1648 cm^{-1} are similar to the normal spectrum (Fig. S2†), and the slight Raman shift is due to the interaction between the probe molecules and the substrate. Another important feature presented in the lower part of Fig. 5 was the excellent reproducibility of the SERS signals. The SERS contour was plotted for a line-mapping mode at a 1 μm increment of 150 spots, and each spot exhibited a distinctive Raman signal. The strong and uniform SERS signals implied that the Au/CuS composite was an excellent substrate with remarkable SERS activity and high reproducibility.

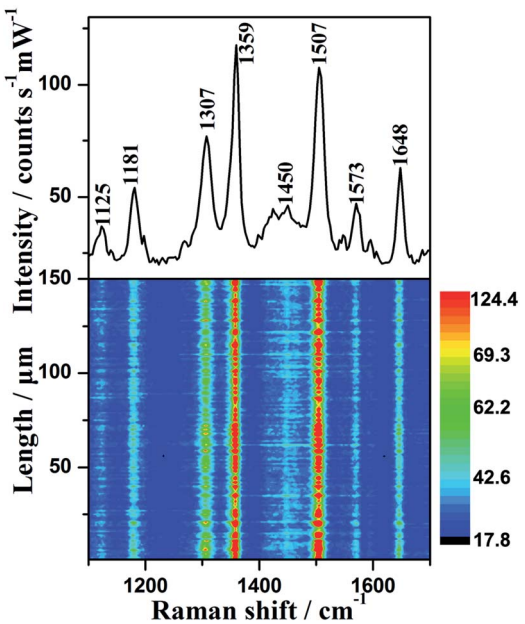

Fig. 5 The Raman spectrum of R6G aqueous solution (1×10^{-6} M) on Au/CuS substrate (upper part) and the SERS contour (lower part).

To quantitatively demonstrate the enhancement, the main peak at 1507 cm^{-1} is employed to calculate the enhancement factor (EF) based on the equation

$$\mathrm{EF} = \frac{I_{\mathrm{SERS}} N_0}{I_0 N_{\mathrm{SERS}}}$$

where I_{SERS} and N_{SERS} are the peak intensity of the Raman and probe molecule number under SERS conditions, respectively. I_0 and N_0 are the peak intensities of the normal Raman and probe molecule number measured in 0.2 M R6G aqueous solution. According to the equation, the EF was calculated to be 2.53×10^5 (details in the ESI†), which confirmed that the Au/CuS substrate showed excellent SERS enhancement for the adsorbed R6G molecules.

In addition, to further semi-quantitatively assess the uniformity of these SERS signals, the relative standard deviation (RSD) of the intensity of the carbon skeleton-stretching modes was calculated and shown in Fig. S3.† The RSD values of the vibrations at 1307, 1359, 1507, and 1648 cm^{-1} were 14.5%, 15.6%, 14.0%, and 13.6%, respectively. An RSD variation of the four bands of less than 20% further demonstrated that the as-prepared Au/CuS composite was a promising substrate with high uniformity.[46]

3.4 The peroxidase-like catalytic activity of Au/CuS composites

It has been reported that CuS nanostructures have intrinsic peroxidase-like activity. Cu^{2+}, similar to Fe^{3+} and Fe^{2+}, is often used as a Fenton-like reagent and also shows peroxidase-like activity similar to Fe_3O_4 and FeS.[30,31]

Here, the peroxidase-like behavior of the as-prepared Au/CuS composites were investigated spectrophotometrically at room temperature through the catalytic oxidation of OPD and DAB in the presence of H_2O_2, which are typically employed as horseradish peroxidase (HRP) substrates. Similar to the enzymatic peroxidase activity observed from the HRP, OPD can be oxidized

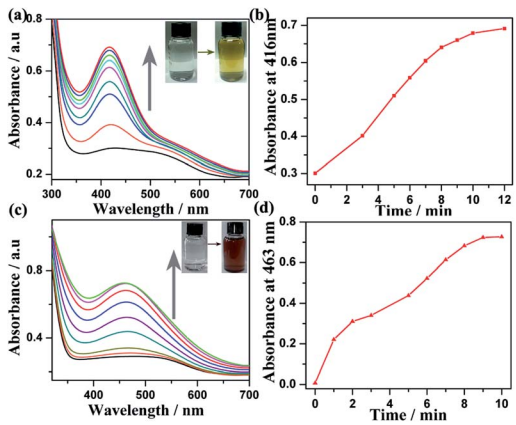

Fig. 6 (a) and (b) are the time-dependent UV-Vis spectra and absorption–time curve at 416 nm in the OPD–H_2O_2 system; (c) and (d) are the time-dependent UV-Vis spectra and absorption–time curve at 463 nm in DAB–H_2O_2 system; in the inset are the typical photographs of OPD and DAB before and after oxidation, respectively.

to a brown reaction product (Fig. 6(a) inset) in the presence of H_2O_2 upon addition of Au/CuS catalysts. The catalytic reaction can be monitored by following the changing of absorbance at 416 nm, which originates from the oxidation products of OPD (Fig. 6(a)). Fig. 6(b) presents the time course curves of the absorbance at 416 nm within 12 min. That the absorbance increased almost linearly with time after the addition of Au/CuS also indicated its high catalytic activity toward OPD oxidation. The controlled experiments were also conducted, and both the system of Au/CuS–OPD and H_2O_2–OPD had no absorbance at 416 nm, which indicated that both Au/CuS and H_2O_2 were required for the catalytic oxidation reaction. The peroxidase-like activity of the Au/CuS composite was further proven by the oxidation of the DAB substrate instead of OPD. From Fig. 6(c) and (d), it also can be observed that the absorbance at 463 nm, which comes from the oxidation products of DAB, increased with the time extension. In addition, the color changed from colorless to reddish-brown, simultaneously. All these tests indicated that Au/CuS composites possessed high peroxidase-like activity toward typical peroxidase substrates (OPD and DAB) in the presence of hydrogen peroxide.

It has been confirmed that the peroxidase-like activity of Fe_3O_4 and FeS nanoparticles originated from the Fenton reactivity of Fe ions.[33,47] Hence, to investigate the catalytic mechanism of the Au/CuS composites, the enzyme-like activity may also originate from the Cu^{2+} ions presenting at the surface of the nanoparticles. Similar to Fe^{3+}, Cu^{2+} may act as a Fenton-like reagent and interact with the substrate to generate the colored products in the presence of H_2O_2. The mechanism most likely follows Fenton's reaction[48,49] and can be expressed as

$$Cu^{2+} + H_2O_2 \rightarrow CuOOH^+ + H^+$$

$$CuOOH^+ \rightarrow Cu^+ + HOO^\bullet$$

$$Cu^+ + H_2O_2 \rightarrow Cu^{2+} + OH^\bullet + OH^-$$

The strong oxidizing hydroxyl radical ($HO^\bullet$), formed during the course of the reaction, may catalyze the oxidation of the OPD and DAB substrates to generate colored products. The generated $HO^\bullet$ radical is a very strong oxidizing agent (standard redox potential +2.8 V) with non-selectivity and the ability to oxidize most of azo dyes to the mineral end-products.[50] Because of this peroxidase-like activity, Au/CuS catalysts can be applied in the degradation of organic pollutants in wastewater systems in the presence of H_2O_2. Moreover, to verify that $OH^\bullet$ was generated in this process, terephthalic acid (TA) was used as photoluminescence probing, which was widely used in the detection of $OH^\bullet$.[51] The obvious fluorescence enhancement after the addition of Au/CuS catalysts strongly suggested that a high amount of $HO^\bullet$ was generated in the catalytic reaction (Fig. S4†).

3.5 *In situ* SERS monitoring of the catalytic degradation of R6G molecules

Based on the above-mentioned experimental results, the Au/CuS substrate exhibited both high peroxidase-like activity and excellent SERS performance. In order to conduct real-time monitoring, the degradation process of organic pollutants with SERS spectroscopy, organic pollutant R6G dye was chosen because it is a common SERS probe molecule and may be degraded into carbon dioxide, water and other small molecules.[14,52]

Quantitative monitoring by SERS is based on a single parameter such as peak intensity or area. This approach can be implemented easily when the corresponding marker bands of the distinct species are spectrally well separated from each other. In this system, the relationship between the peak intensity and the concentration of R6G molecules is displayed in Fig. S5,† corresponding to the linear relationship in the range of 1×10^{-7} to 2×10^{-5} M. The peaks at 1359 cm^{-1} and 1507 cm^{-1} corresponding to aromatic C–C stretching can also be chosen as marker peaks, and the linear relationships are expressed as $I_{R6G} = 1.209 \times 10^7 C_{R6G} + 12.90$ and $I_{R6G} = 1.168 \times 10^7 C_{R6G} + 10.58$, respectively. Therefore, the peak intensity may be transformed into the corresponding concentration.

SERS monitoring measurements were performed in a liquid system as shown in Fig. 7(a) using a 633 nm laser. Fig. 7(b) ($t = 0$) shows the SERS spectrum of R6G molecules on the surface of the Au/CuS substrate. The catalytic reaction was initiated by adding diluted H_2O_2 to the solution. The degradation process was monitored *in situ* by collecting the SERS signal directly from the surface of Au/CuS substrates. The Raman intensity of the characteristic peaks of R6G molecules gradually decreased with increasing time without the emergence of new bands, which indicated the degradation of the R6G molecules. After 8 min of degradation reaction, the main peaks of R6G almost disappeared.

To determine the kinetic parameters accurately, the linear relationship of ln C (C is the concentration of R6G) with a reaction time obtained from SERS spectra is displayed in Fig. 7(c) and (d). The plots of ln C *versus* time for the two SERS bands (1359 cm^{-1} and 1507 cm^{-1}) show a linear relationship, which can be expressed as $\ln C = -0.2756t + 5.3351$ and $\ln C = -0.3525t + 5.3211$, respectively. These results proved that the degradation of R6G by adding H_2O_2 followed pseudo-first-order

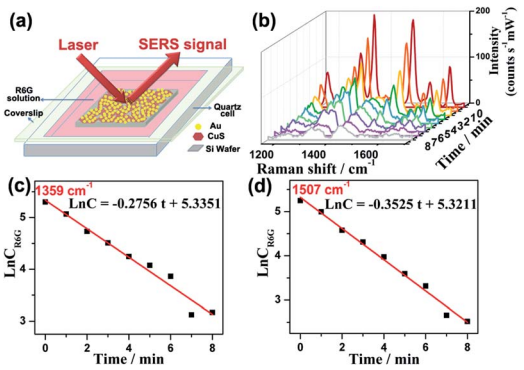

Fig. 7 (a) Schematic of *in situ* SERS monitoring of R6G degradation on the Au/CuS substrates; (b) the changing of Raman spectra in the process of the degradation of R6G molecules on Au/CuS substrates; (c) and (d) the linear relationship between the R6G concentration and degradation time according to the peaks at 1359 and 1507 cm^{-1}, respectively.

kinetics. The rate constants calculated from the slopes of the straight lines were 0.2756 and 0.3525, respectively. It is reported that if R6G is oxidised and the concentration is reduced, the Langmuir adsorption is also expected to change. SERS intensity was found to correlate linearly with concentration only in a saturation of very low surface coverage.[41] Here, the linear relationship between intensity and concentration was in the range of 1×10^{-7} to 2×10^{-5} M, and therefore, the degradation was conducted with the initial concentration of R6G of 2×10^{-5} M.

4. Conclusions

In conclusion, the prepared Au/CuS composites have been found to possess peroxidase-like activity to catalyze the oxidation of typical peroxidase substrates (OPD and DAB) in the presence of hydrogen peroxide. The strong oxidizing hydroxyl radical ($HO^{\bullet}$), formed in the process of a catalytic reaction, could be exploited to degrade most of the organic pollutants. Moreover, the Au/CuS composites were also demonstrated to be an excellent SERS substrate with remarkable sensitivity and high reproducibility. Based on the bifunctional behaviors of catalytic activity and SERS performance, the Au/CuS substrate was employed both as a catalyst for degrading pollutants (R6G) and a SERS substrate for real-time monitoring of the degradation quantitatively. More importantly, SERS monitoring could be applied for capturing and enriching reactants on the surfaces of substrates, which more accurately revealed the catalytic reaction. Thus, it is worthwhile to design more multi-functional metal/semiconductor composites, which can be applied in potential fields, such as environmental monitoring and biological indicators.

Acknowledgements

The project was supported by the National Basic Research Program of China (973 Program) (Grant no. 2012CB932903, 2010CB934502), the Innovative Research Teams of Jiangsu Higher Education Institutions, and the Priority Academic Program Development of Jiangsu Higher Education Institutions.

Notes and references

1 I. Udom, M. K. Ram, E. K. Stefanakos, A. F. Hepp and D. Y. Goswami, *Mater. Sci. Semicond. Process.*, 2013, **16**, 2070.
2 P. Collier and C. M. Alles, *Science*, 2010, **330**, 919.
3 Y. B. Wang, Y. N. Zhang, G. H. Zhao, H. Y. Tian, H. J. Shi and T. C. Zhou, *ACS Appl. Mater. Interfaces*, 2012, **4**, 3965.
4 W. Cheung, I. T. Shadi, Y. Xu and R. Goodacre, *J. Phys. Chem. C*, 2010, **114**, 7285.
5 X. Zhuang, Y. Wan, C. M. Feng, Y. Shen and D. Y. Zhao, *Chem. Mater.*, 2009, **21**, 706.
6 C. H. Wu and J. M. Chern, *Ind. Eng. Chem. Res.*, 2006, **45**, 6450.
7 J. Ge and J. Qu, *Appl. Catal., B*, 2004, **47**, 133.
8 X. H. Li, G. Y. Chen, L. B. Yang, Z. Jin and J. H. Liu, *Adv. Funct. Mater.*, 2010, **20**, 2815.
9 M. Tokumura, T. Katoh, H. Ohata and Y. Kawase, *Ind. Eng. Chem. Res.*, 2009, **48**, 7965.
10 A. Y. Satoh, J. E. Trosko and S. J. Masten, *Environ. Sci. Technol.*, 2007, **41**, 2881.
11 Z. Li, L. Mi, W. Chen, H. Hou, C. Liu and H. Wang, *CrystEngComm*, 2012, **14**, 3965.
12 Y. Li, H. Zhang, Z. Guo, J. Han, X. Zhao, Q. Zhao and S. J. Kim, *Langmuir*, 2008, **24**, 8351.
13 W. J. Zhou, H. Liu, J. Y. Wang, D. Liu, G. J. Du and J. J. Cui, *ACS Appl. Mater. Interfaces*, 2010, **2**, 2385.
14 X. Zhao, B. Zhang, K. Ai, G. Zhang, L. Cao, X. Liu and L. Lu, *J. Mater. Chem.*, 2009, **19**, 5547.
15 Y. Ma, Q. Ding, L. Yang, L. Zhang and Y. Shen, *Appl. Surf. Sci.*, 2013, **265**, 346.
16 M. D. Porter, R. J. Lipert, L. M. Siperko, G. Wang and R. Narayanan, *Chem. Soc. Rev.*, 2008, **37**, 1001.
17 X. Qian, X. Zhou and S. Nie, *J. Am. Chem. Soc.*, 2008, **130**, 14934.
18 W. Xie, B. Walkenfort and S. Schlücker, *J. Am. Chem. Soc.*, 2012, **135**, 1657.
19 C. Y. Wen, F. Liao, S. S. Liu, Y. Zhao, Z. H. Kang, X. L. Zhang and M. W. Shao, *Chem. Commun.*, 2013, **49**, 3049.
20 H. Li, Z. Bian, J. Zhu, Y. Huo, H. Li and Y. Lu, *J. Am. Chem. Soc.*, 2007, **129**, 4538.
21 C. J. Zhong and M. M. Maye, *Adv. Mater.*, 2001, **13**, 1507.
22 A. Chou, B. Radi, E. Jaatinen, S. Juodkazis and P. Fredericks, *Analyst*, 2014, **139**, 1960.
23 T. Hutter, S. R. Elliott and S. Mahajan, *Nanotechnology*, 2013, **24**, 035201.
24 M. W. Knight, Y. Wu, J. B. Lassiter, P. Nordlander and N. J. Halas, *Nano Lett.*, 2009, **9**, 2188.
25 J. Ye, F. Wen, H. Sobhani, J. B. Lassiter, P. V. Dorpe, P. Nordlander and N. J. Halas, *Nano Lett.*, 2012, **12**, 1660.
26 R. H. Que, M. W. Shao, S. J. Zhuo, C. Y. Wen, S. D. Wang and S. T. Lee, *Adv. Funct. Mater.*, 2011, **21**, 3337.
27 J. Yu, J. Zhang and S. Liu, *J. Phys. Chem. C*, 2010, **114**, 13642.
28 H. Lee, S. W. Yoon, E. J. Kim and J. Park, *Nano Lett.*, 2007, **7**, 778.
29 A. B. F. Martinson, J. W. Elam and M. J. Pellin, *Appl. Phys. Lett.*, 2009, **94**, 123107.
30 X. Zhang, G. Wang, A. Gu, Y. Wei and B. Fang, *Chem. Commun.*, 2008, 5945.
31 W. He, H. Jia, X. Li, Y. Lei, J. Li, H. Zhao and Z. Zheng, *Nanoscale*, 2012, **4**, 3501.
32 H. Wei and E. Wang, *Anal. Chem.*, 2008, **80**, 2250.
33 L. Gao, J. Zhuang, L. Nie, J. Zhang, Y. Zhang, N. Gu and X. Yan, *Nat. Nanotechnol.*, 2007, **2**, 577.
34 A. Santos, P. Yustos, S. Rodriguez, E. Simon and A. Romero, *Ind. Eng. Chem. Res.*, 2010, **49**, 5583.
35 J. Jiang, J. Zou, L. Zhu, L. Huang, H. Jiang and Y. Zhang, *J. Nanosci. Nanotechnol.*, 2011, **11**, 4793.
36 D. D. Gates and R. L. Siegrist, *J. Environ. Eng.*, 1995, **121**, 639.
37 G. Gervinskas, G. Seniutinas, J. S. Hartley, S. Kandasamy, P. R. Stoddart, N. F. Fahim and S. Juodkazis, *Ann. Phys.*, 2013, **525**, 907.
38 F. Liao, S. S. Liu, M. W. Shao and S. T. Lee, *Appl. Phys. Lett.*, 2012, **100**, 093114.
39 F. H. Chung, *J. Appl. Crystallogr.*, 1974, **7**, 519.

40 Z. L. Yang, Q. Li, F. Ruan, Z. Li, B. Ren, H. Xu and Z. Q. Tian, *Chin. Sci. Bull.*, 2010, **55**, 2635.
41 Y. Yokota, K. Ueno, S. Juodkazis, V. Mizeikis, N. Murazawa, H. Misawa and J. Nishii, *J. Photochem. Photobiol., A*, 2009, **207**, 126.
42 E. Güneri and A. Kariper, *J. Alloys Compd.*, 2012, **516**, 20.
43 M. Ali Yildirim, *Opt. Commun.*, 2012, **285**, 1215.
44 Y. Cao, D. Li, F. Jiang, Y. Yang and Z. Huang, *J. Nanomater.*, 2013, **2013**, 123812.
45 M. W. Shao, L. Lu and H. Wang, *Chem. Commun.*, 2008, 2310.
46 H. Liang, Z. Li, W. Wang, Y. Wu and H. Xu, *Adv. Mater.*, 2009, **21**, 4614.
47 M. Ma, J. Xie, Y. Zhang, Z. Chen and N. Gu, *Mater. Lett.*, 2013, **105**, 36.
48 J. F. Perez-Benito, *J. Phys. Chem. A*, 2004, **108**, 4853.
49 Z. Chen, J. J. Yin, Y. T. Zhou, Y. Zhang, L. Song, M. Song and N. Gu, *ACS Nano*, 2012, **6**, 4001.
50 I. K. Konstantinou and T. A. Albanis, *Appl. Catal., B*, 2004, **49**, 1.
51 H. Li, R. Liu, S. Lian, Y. Liu, H. Huang and Z. Kang, *Nanoscale*, 2013, **5**, 3289.
52 A. Mills and S. Le Hunte, *J. Photochem. Photobiol., A*, 1997, **108**, 1.